Biochimica et Biophysica Acta 1827 (2013) 658–667

Contents lists available at SciVerse ScienceDirect

Biochimica et Biophysica Acta

journal homepage: www.elsevier.com/locate/bbabio

Review

# Diversity of parasite complex II☆

Shigeharu Harada [a,*], Daniel Ken Inaoka [b], Junko Ohmori [b], Kiyoshi Kita [b,**]

[a] Department of Applied Biology, Graduate School of Science and Technology, Kyoto Institute of Technology, Kyoto 606-8585, Japan
[b] Department of Biomedical Chemistry, Graduate School of Medicine, The University of Tokyo, Tokyo 113-0033, Japan

ARTICLE INFO

*Article history:*
Received 16 October 2012
Received in revised form 7 January 2013
Accepted 9 January 2013
Available online 16 January 2013

*Keywords:*
Complex II
Fumarate respiration
*Ascaris suum*
*Trypanosoma cruzi*
Chemotherapy
Drug design

ABSTRACT

Parasites have developed a variety of physiological functions necessary for completing at least part of their life cycles in the specialized environments of surrounding the parasites in the host. Regarding energy metabolism, which is essential for survival, parasites adapt to the low oxygen environment in mammalian hosts by using metabolic systems that are very different from those of the hosts. In many cases, the parasite employs aerobic metabolism during the free-living stage outside the host but undergoes major changes in developmental control and environmental adaptation to switch to anaerobic energy metabolism. Parasite mitochondria play diverse roles in their energy metabolism, and in recent studies of the parasitic nematode, *Ascaris suum*, the mitochondrial complex II plays an important role in anaerobic energy metabolism of parasites inhabiting hosts by acting as a quinol-fumarate reductase. In Trypanosomes, parasite complex II has been found to have a novel function and structure. Complex II of *Trypanosoma cruzi* is an unusual supramolecular complex with a heterodimeric iron–sulfur subunit and seven additional non-catalytic subunits. The enzyme shows reduced binding affinities for both substrates and inhibitors. Interestingly, this structural organization is conserved in all trypanosomatids. Since the properties of complex II differ across a wide range of parasites, this complex is a potential target for the development of new chemotherapeutic agents. In this regard, structural information on the target enzyme is essential for the molecular design of drugs. This article is part of a Special Issue entitled: Respiratory complex II: Role in cellular physiology and disease.



## 1. Introduction

### 1.1. Molecular parasitology

Parasites are classified generally as either helminths or protozoans. Helminths are multi-cellular parasites and are divided into three types: nematodes (e.g., *Ascaris suum*), trematodes (e.g., *Schistosoma japonica*), and cestodes (e.g., *Diphyllobothrium latum*). Protozoans include unicellular parasites (e.g., malaria parasites and *Entamoeba histolytica*), but they differ from bacteria in that they have a nucleus, mitochondria, vacuole, and other organelles (e.g., apicoplast, hydrogenosomes, and mitosomes). These parasites are capable of surviving and proliferating due to avoidance of host defense mechanisms and development of metabolic pathways adapted to the specialized environments of the host [see reviews 1–5].

Studies of parasitic adaptation have yielded extremely informative biological discoveries and data that are potentially useful for developing treatments of infectious diseases. Recent advances in biochemistry and molecular biology have provided new insights into basic parasite biology and have led to many revolutionary discoveries concerning biological evolution and diversity. Taken together, a new field called 'molecular parasitology' is being established to investigate parasitism at the molecular level. The unique features of parasite complex II have been revealed through data obtained through such a pioneering sciences [1,4,5].

### 1.2. Functional and subunit changes of complex II during the A. suum life cycle

The nematode *A. suum* has been studied extensively as a representative of human and livestock parasites [1]. During its life cycle, *A. suum* transitions from aerobic to anaerobic metabolism, reflecting the change in the environmental oxygen concentration (Fig. 1) [2–7]. During development from a fertilized egg to third stage larvae (L3) outside of the host, metabolism is aerobic as the tissues of mammalian host in that ATP is synthesized by aerobic oxidative phosphorylation [8]. In contrast,

*Abbreviations:* PEPCK, phosphoenolpyruvate carboxykinase; RQ, rhodoquinone; QFR, quinol-fumarate reductase; Fp, flavoprotein; FAD, flavin adenine dinucleotide; Ip, iron–sulfur protein; CybL, large subunit ofcytochrome *b*; CybS, small subunit of cytochrome *b*; SDH, succinate dehydrogenase; UQ, ubiquinone; SQR, succinate-ubiquinone reductase; MK, menaquinone; $RQH_2$, rhodoquinol; FRD, fumarate reductase; OAA, oxaloacetate

☆ This article is part of a Special Issue entitled: Respiratory complex II: Role in cellular physiology and disease.

* Correspondence to: S. Harada, Department of Applied Biology, Graduate School of Science and Technology, Kyoto Institute of Technology, Sakyo-ku, Kyoto 606-8585, Japan. Tel.: +81 75 724 7541; fax: +81 75 724 7541.
** Correspondence to: K. Kita, Department of Biomedical Chemistry, Graduate School of Medicine, The University of Tokyo, Hongo, Bunkyo-ku, Tokyo 113-0033, Japan. Tel.: +81 3 5841 3526; fax: +81 3 5841 3444.
*E-mail addresses:* harada@kit.ac.jp (S. Harada), kitak@m.u-tokyo.ac.jp (K. Kita).

0005-2728/$ – see front matter © 2013 Published by Elsevier B.V.
http://dx.doi.org/10.1016/j.bbabio.2013.01.005

adult worms, which live in a low-oxygen environment, use the anaerobic phosphoenolpyruvate carboxykinase (PEPCK)-succinate pathway. The last step of the PEPCK-succinate pathway involves the NADH-fumarate reductase system, which is composed of complex I (NADH-quinone reductase), low-potential rhodoquinone (RQ), and complex II (quinol-fumarate reductase, QFR) [4,9]. Electron transfer from NADH to fumarate is coupled to ATP synthesis by site I phosphorylation in complex I. The difference in redox potential between $NAD^+$/NADH ($E$m' = −320 mV) and fumarate/succinate ($E$m' = +30 mV) is sufficient to drive ATP synthesis [4].

In eukaryotes, complex II is localized in the inner mitochondrial membrane and is generally composed of four peptides [4]. The largest flavoprotein (Fp, SDHA) subunit has a molecular mass of about 70 kDa and contains flavin adenine dinucleotide (FAD) as a prosthetic group. The relatively hydrophilic catalytic region of complex II is formed by the Fp subunit and the iron–sulfur cluster (Ip, SDHB) subunit, which has a molecular weight of about 30 kDa. The remaining subunits comprise cytochrome *b*, which contains heme *b*. Cytochrome *b* is composed of 2 hydrophobic membrane-anchoring polypeptide subunits: the 15 kDa large subunit (CybL, SDHC) and the 13 kDa small subunit (CybS, SDHD). These cytochrome *b* subunits are necessary for the interaction between complex II and hydrophobic membrane-associated quinones, such as ubiquinone (UQ) and RQ [6].

In a previous study, we showed that *A. suum* mitochondria express stage-specific isoforms of complex II [6,7,10]. While there are no differences in the isoforms of the Ip and CybL subunits of complex II between L3 larvae and adult *A. suum*, there are different isoforms of the complex II subunits Fp (larval, $Fp^L$; adult, $Fp^A$) and CybS (larval, $CybS^L$; adult, $CybS^A$) [7]. Quinone species in the mitochondria also differ during the life cycle of *A. suum*. In the adult mitochondria, the predominant quinone is the low-potential RQ ($E$m' = −63 mV); in larvae, the predominant quinone is UQ ($E$m' = +110 mV) [11]. Similarly, *Escherichia coli* and other bacteria show shifts in the combination of succinate-ubiquinone reductase (SQR) and UQ, and that of QFR and a low-potential quinone, such as menaquinone (MK) or RQ, during metabolic adaptation to changes in oxygen supply [12,13]. UQ has a higher redox potential than RQ; therefore, RQ is better suited to transferring electrons to fumarate than is UQ. In L2 and L3 *A. suum* larvae, UQ preferentially donates electrons to the cytochrome chain in the mitochondria. Thus, UQ participates in aerobic metabolism in *A. suum* larvae, whereas RQ participates in anaerobic metabolism in adult *A. suum* [11].

After being ingested by the definitive host, the L3 larvae penetrate the intestinal wall and reach the lung by migrating through other tissues, such as liver and heart. The L3 larvae pass from the lung via the trachea to the small intestine where they molt to L4 and develop into sexually maturate adult worms in the small intestine [14]. Protein chemical analysis reveals that the change in complex II begins with the anchor CybS subunit and then the Fp subunit [15].

### 1.3. Parasite complex II

Complex II molecules are classified into four types (Type A–D) and three classes (Class 1–3) according to the architecture of membrane anchors and functions *in vivo*, respectively [16]. The membrane anchor of Type A complex II consists of two polypeptide chains each having three transmembrane helices and two protoheme IX (heme *b*) molecules. Type B has one polypeptide chain with five transmembrane helices and two heme *b* molecules. On the other hand, Type C and D, like Type A, consist of two polypeptide chains with one and no heme *b* molecules in their anchors, respectively. In addition, more recent physiological analysis indicates novel Type E complex II [17], which is different from Type A–D in membrane-anchoring subunits and the composition of iron–sulfur centers. Class 1 complex II functions as SQR *in vivo* and catalyzes the oxidation of succinate and the reduction of high potential quinone, typically ubiquinone, whereas Class 2 complex II (QFR) catalyzes the opposite reaction, the oxidation of low potential quinol such as menaquinol and rhodoquinol ($RQH_2$) and the reduction of fumarate. Complex II belonging to Class 3, like the Class 1 enzymes, exhibits SQR activity but reduces low potential quinone. Crystal structures of complex II have been determined for three QFRs from *E. coli* (pdb code, 1L0V; [18]), *Wolinella succinogenes* (1QLB; [19]) and *A. suum* (3VR8; [20]), three SQRs from *E. coli* (1NEK; [21]), porcine (1ZOY; [22]) and chicken (1YQ3; [23]). QFRs from *E. coli*, *W. succinogenes*, and *A. suum* belong to Type D, Type B and Type C,

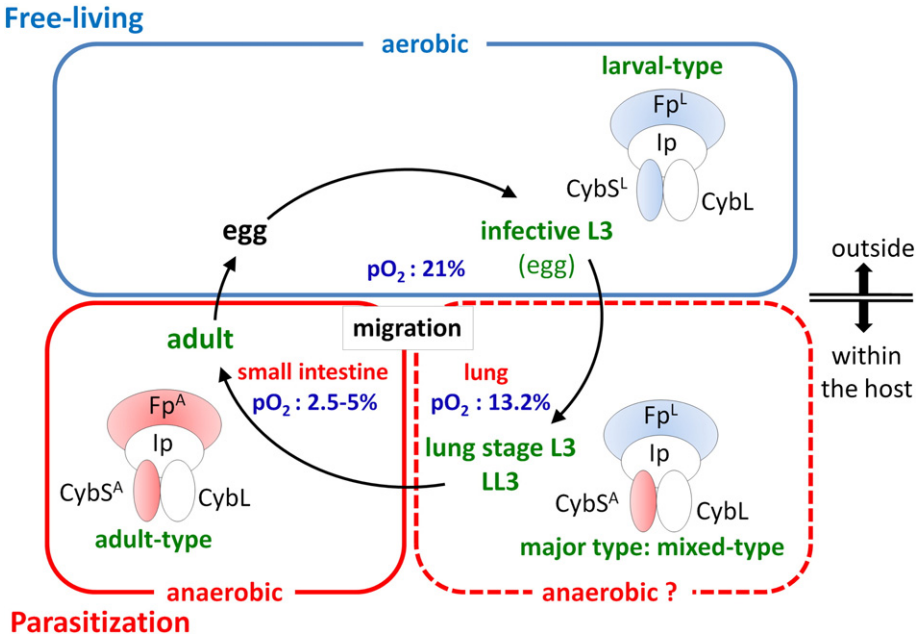


**Fig. 1.** Life cycle of *A. suum*. Fertilized eggs grow to infective L3 under an aerobic environment. Infective L3 larvae are ingested by the host, reach the small intestine and hatch there. Afterwards, larvae migrate into the host body (liver, heart, lung, and pharynx), and finally migrate back to the small intestine and develop into adults. In the host small intestine, the oxygen concentration is only 2.5% to 5% of that of the exogenous environment. During the life cycle, complex II molecules are expressed as stage-specific isoforms, larval-type, mixed-type and adult-type [15].

respectively, whereas SQRs from porcine, chicken and *E. coli* are the Type C enzymes.

In general, the complex II molecules of helminthes, which are multi-cellular parasites, are of Type C, although catalytic function changes during the life cycle as mentioned above. However, complex II purified from the parasitic protist, *Trypanosoma cruzi*, consists of six hydrophilic and six hydrophobic nuclear-encoded subunits [24]. Notably, the iron–sulfur subunit is heterodimeric; $SDH2_N$ and $SDH2_C$ contain plant-type ferredoxin domains in the *N*-terminal half and bacterial ferredoxin domains in the C-terminal half, respectively.

In the case of malaria parasites, such as *Plasmodium falciparum*, anchor subunits of complex II have not yet been identified, although the enzyme shows SQR activity [25]. These unusual features of parasite complex II molecules make them targets for new chemotherapeutic agents.

In this review, we mainly focus on recent advances in the study of *A. suum* complex II, which plays an important role in the anaerobic energy metabolism of parasites. In addition, the molecular architecture of 12 novel complex II subunits of *T. cruzi* will be discussed.

## 2. Structure of adult *A. suum* QFR

Anaerobic mitochondrial complex II from adult *A. suum* (*A. suum* QFR) belongs to Type C/Class 2 and couples the oxidation of $RQH_2$ to RQ to the reduction of fumarate to succinate, an opposite reaction catalyzed by SQR of the aerobic respiratory chain [7]. We crystallized *A. suum* QFR in the presence of malonate [26], a well-known competitive inhibitor against complex II in various organisms and determined the crystal structure at 2.8 Å resolution (3VR8; [20]) by molecular replacement using the structure of porcine SQR (1ZOY; [22]) as the search model. In addition, the structure of the ternary complex with fumarate and flutolanil was determined at 2.9 Å resolution (3VRB; [20]). Flutolanil is a widely used commercially available fungicide [27] that specifically inhibits *A. suum* QFR as shown by $IC_{50}$ values for *A. suum* QFR of 58 nM and porcine SQR of 46 μM. Based on these structures, as well as the structure of porcine SQR in complex with flutolanil (3AE8), the enzymatic mechanism of *A. suum* QFR and the structural basis of the specificity of flutolanil against *A. suum* QFR will be discussed.

### 2.1. Overall structure

The structure of *A. suum* QFR, the first eukaryotic Type C/Class 2 complex II molecule to be characterized, is composed of four protein subunits (Fig. 2A): hydrophilic Fp (residues A33–A645) and Ip (B33–B281) subunits, and membrane-anchoring hydrophobic CybL (C34–C186) and CybS (D28–D156) subunits [20]. Several terminal residues of each mature polypeptide (Fp: A31–A645, Ip: B29–B282, CybL: C32–C188 and CybS: D26–D156) are missing in the current model because of faint electron density. The enzyme accommodates five prosthetic groups: a FAD molecule, three ion-sulfur centers ([2Fe–2S], [4Fe–4S], [3Fe–4S]), and one heme *b* molecule (Fig. 2B). Although there are two molecules in the asymmetric unit, *A. suum* QFR, like *E. coli* QFR [18], porcine SQR [22] and chicken SQR [23], exists as a monomer both in solution and crystal, which distinguishes the enzyme from the reported dimer structure of *W. succinogenes* QFR [19] and the trimer structure of *E. coli* SQR [21]. Further, the amino acid sequence of each subunit of *A. suum* QFR (Fig. 3) shows higher identity with porcine and chicken SQRs than with *E. coli* SQR and *E. coli* and *W. succinogenes* QFRs. Accordingly, *A. suum* QFR is more closely related to porcine and chicken SQRs rather to *E. coli* and *W. succinogenes* bacterial complex IIs. The arrangement of the bound prosthetic groups in the *A. suum* QFR structure [20] is similar to that of other complex IIs with known structures [18,19,21–23]. The chain of the FAD, [2Fe–2S], [4Fe–4S] and [3Fe–4S] prosthetic groups is disposed between dicarboxylate- and quinone-binding sites with the distances between neighboring centers less than 14 Å (Fig. 2B), suggesting that electron transfer from $RQH_2$ to FAD is carried out by quantum tunneling [28], as proposed for *E. coli* SQR [21].

### 2.2. Fp subunit

The largest Fp subunit of *A. suum* QFR [20] folds into four domains (Fig. 4A): a FAD-binding domain (residues A33–A280 and A380–A465), a capping domain (A281–A379), a helical domain (A466–A568), and a C-terminal domain (A569–A645). The FAD molecule forms a covalent bond with His A79 and hydrogen bonds primarily with main-chain N atoms of highly conserved residues of the FAD-binding domain (A49, A71, A72, A73, A78, A80, A84, A85, A86, A201, A255, A421, A432, A437 and A438). In addition, residues within 5 Å of the FAD group, especially those close to the FAD isoalloxazine ring, are highly conserved (Fig. 3A).

Examination of the refined structure shows significant electron density near the isoalloxazine ring that can be assigned as malonate, an additive for crystallization [20]. The location of this site is in agreement with the dicarboxylate-binding site assigned to other complex IIs with known structures [18,19,21–23] and is constructed by residues of the FAD-binding domain (A84, A85, A153, A276, A387, A432 and A435) and the capping domain (A286, A288, A289 and A320). Three basic residues, Arg A320, His A387 and Arg A432, interact with the C3 carboxylate group of the bound malonate, and Thr A288 and Arg A320 with the C1 carboxylate group (Fig. 4A). With the exception of A84, A153 and A435, these residues are conserved across complex II molecules with known structures (Fig. 3A).

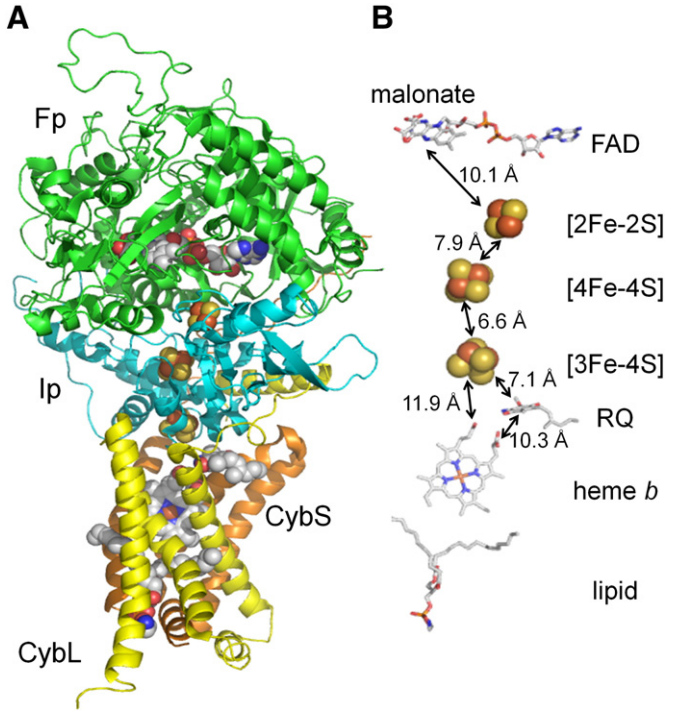


**Fig. 2.** Overall structure of *A. suum* QFR. (A) Cartoon representation of the overall structure of *A. suum* QFR. FAD-binding subunit (Fp) is shown in green; iron–sulfur subunit (Ip) is shown in cyan; and the transmembrane subunits CybL and CybS are shown in yellow and orange, respectively. The intrinsic redox centers (FAD, [2Fe–2S], [4Fe–4S], [3Fe–4S] and heme *b*) and bound small molecules (malonate, rhodoquinone, and lipid) are shown as spheres. (B) The arrangement of the redox centers together with malonate, rhodoquinone and lipid, and edge-to-edge distances between adjacent redox centers. For calculation of edge-to-edge distances, the dominant determinants of the electron tunneling rate, the sulfur atoms of the cysteine residues ligating to the iron–sulfur centers are included as part of the redox centers. The FAD edge is the isoalloxazine ring system and the heme edge is the conjugated macrocycle. Color-coding for each atom type is as follows: C, white; N, blue; O, red; S, dark yellow; and Fe, brown.

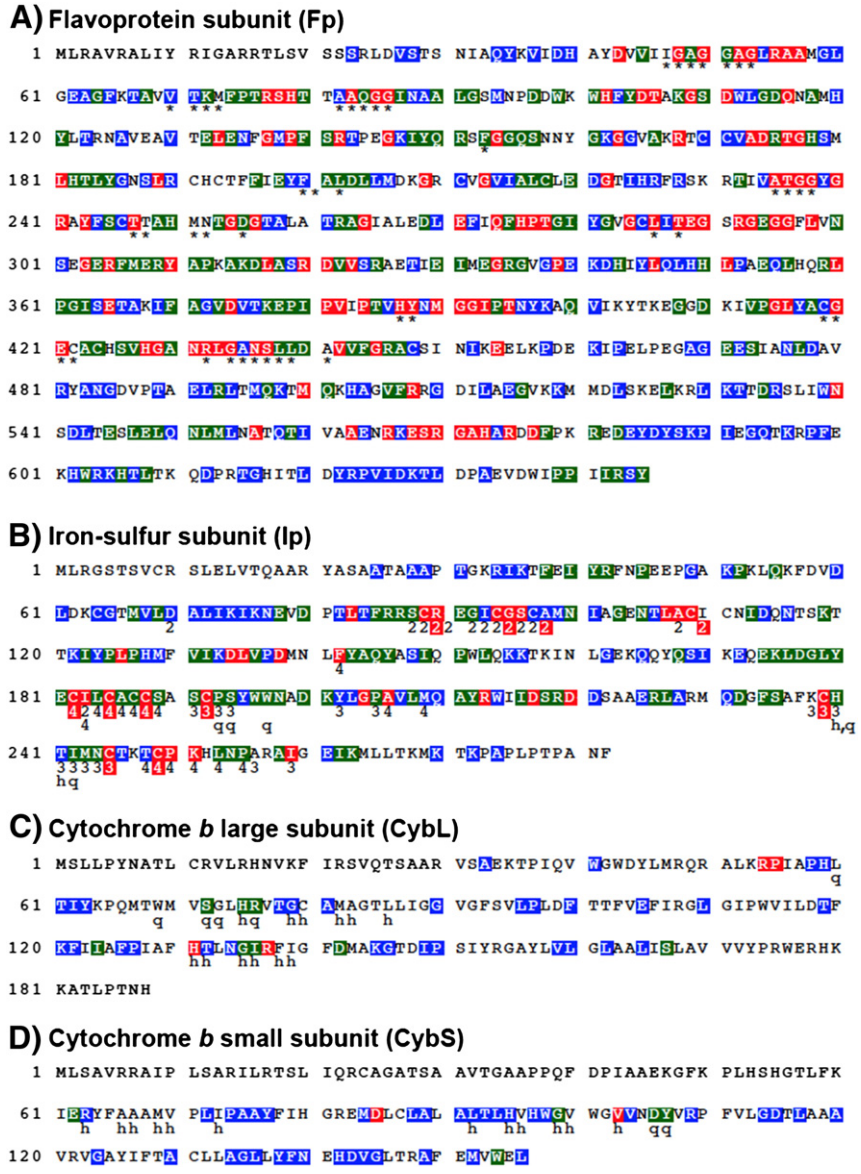


**Fig. 3.** Amino acid sequences of *A. suum* SQR. (A) Fp, (B) Ip, (C) CybL, and (D) CybS subunits. Residues conserved in the six complex II molecules with known structures (SQRs from porcine, chicken, and *E. coli* and QFRs from *E. coli*, *W. succinogenes*, and *A. suum*) are highlighted in red, residues conserved in SQRs from porcine, chicken, and *E. coli* and *A. suum* QFR are highlighted in green, residues conserved in porcine and chicken SQRs and *A. suum* QFR are highlighted in blue. Residues within 5 Å of FAD, [2Fe–2S], [4Fe–4S], [3Fe–4S], rhodoquinone and heme *b* redox centers are marked by *, 2, 4, 3, q, and h, respectively.

### 2.3. Ip subunit

The Ip subunit (Fig. 4B) is constructed by two domains, a plant ferredoxin-like N-terminal (B33–B130) and a bacterial ferredoxin-like C-terminal (B131–B281) domain [20]. The [2Fe–2S] center is bound to the N-terminal domain through coordination bonds with four cysteine residues (B89, B94, B97, and B109). The [4Fe–4S] and [3Fe–4S] centers are bound to the C-terminal domain and are coordinated by four (B182, B185, B188, and B249) and three (B192, B239, and B245) cysteine residues, respectively. Except for Cys B97, which is replaced by aspartate (Asp B63) in *E. coli* SQR [21], the cysteine residues are conserved (Fig. 3B). Out of 47 residues located within 5 Å of the iron–sulfur center of *A. suum* QFR [20], 44 residues are conserved in porcine and chicken SQRs, but that number decreases to 20 residues when compared across all complex II molecules with known structures [18,19,21–23]. The sulfur atoms of the cysteine ligands of [2Fe–2S] and [4Fe–4S] form –S:···H–N< interactions with main-chain amino groups of the N-terminal domain (B91, B92, B93, B96, and B108) and C-terminal domain (B184, B186, B187, B189, and B251), respectively. In addition, sulfur atoms of the iron–sulfur centers interact with the Ip subunit: the [2Fe–2S] center interacts with B90 N and B95 N, the [4Fe–4S] center with B183 N and B186 N, and the [3Fe–4S] center with B243 N. The –S:···H–N< interaction is also found in other complex II molecules [18, 19, 21–23, pdb code: 1L0V, 1QLB, 1NEK, 1ZOY and 1YQ3] and could affect the basicity of sulfur atoms of the cysteine ligands and the redox centers. It is worth noting that side chain atoms of Ser B96, Cys B187, and Tyr B202 interact with sulfur atoms of Cys B94, Cys B185, and [3Fe–4S], respectively (Fig. 4B). Although these residues are conserved in porcine and chicken complex II molecules (Fig. 3), Cys B187 is replaced by Leu in *E. coli* QFR, and Tyr B202 is replaced by Phe in *E. coli* and *W. succinogenes* QFRs and *E. coli* SQR. Therefore, *A. suum* QFR is more similar to mitochondrial porcine and chicken SQRs than bacterial complex II molecules with respect to the environment of the iron–sulfur centers.

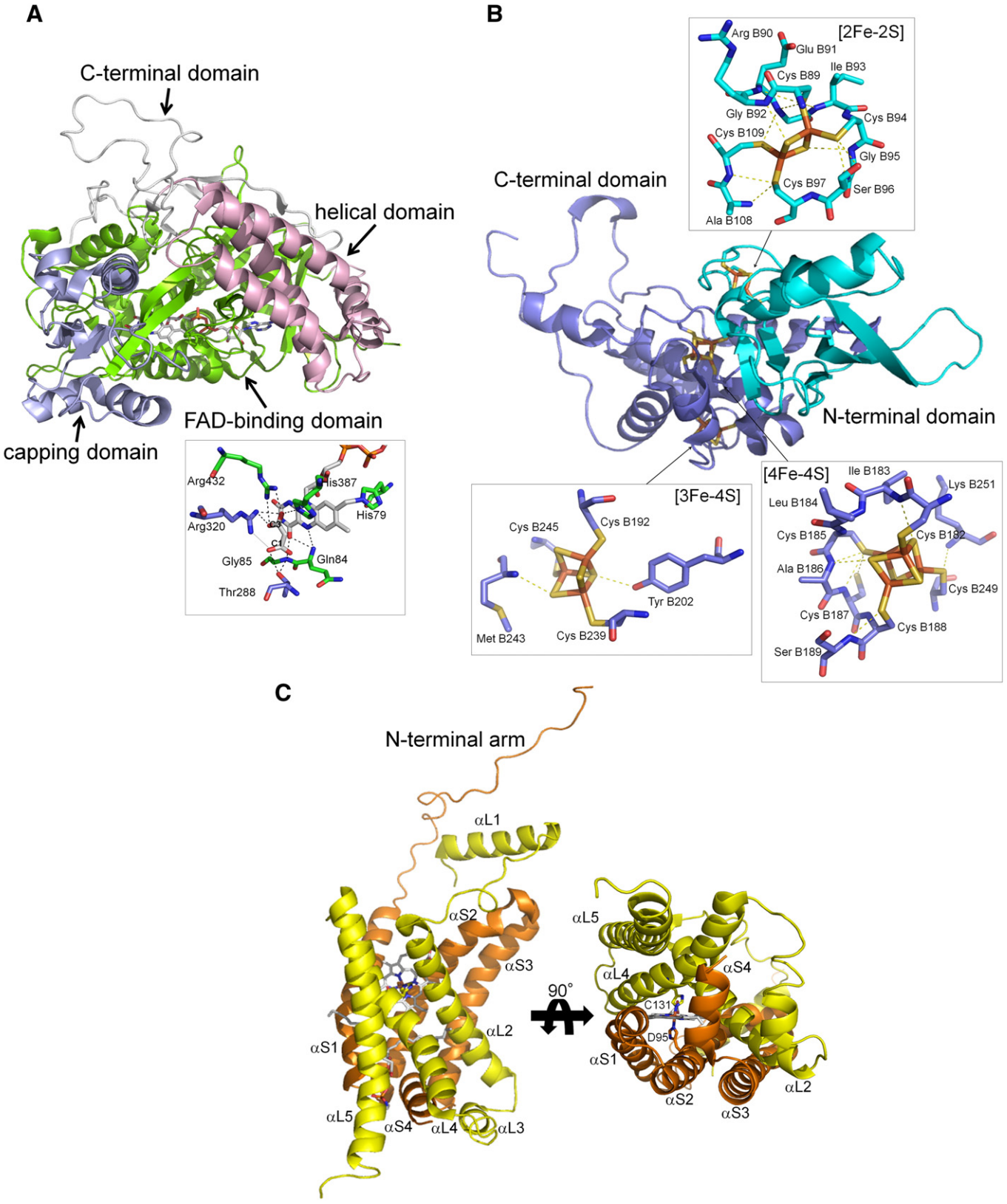


**Fig. 4.** Depiction of subunits. (A) Cartoon representation of the Fp subunit. The FAD-binding domain, capping domain, helical domain and C-terminal domain are shown in pale green, light blue, light pink and white, respectively, together with the stick models of FAD and malonate. The close-up view of the neighborhood of FAD is also represented in the inset. Color-coding for each atom type: C, white; N, blue; and O, red. Carbon atoms of residues from the FAD-binding domain and capping domain are shown in pale green and light blue, respectively. (B) Cartoon representation of the N-terminal domain (cyan) and C-terminal domain (light blue) of the Ip subunit together with the iron–sulfur centers shown as stick models. The close-up view of the iron–sulfur centers, cysteine ligands and residues interacting with the centers are shown in the insets. In (A) and (B), hydrogen bonds are shown with dashed lines. (C) Cartoon representation of the membrane-anchoring CybL (yellow) and CybS (orange) subunits together with heme *b* and the bound lipid molecule viewed from orientations perpendicular to each other. C131 and D95 are histidine residues from CybL and CybS subunits, respectively.

### 2.4. Transmembrane CybL and CybS subunits

The membrane anchor of *A. suum* QFR, like *E. coli*, porcine and chicken SQRs [21–23], is made up of CybL and CybS subunits. They are composed of five (CybL: αL1–αL5) and four (CybS: αS1–αS4) α-helices, of which αL2, αL4, αL5, αS1, αS2, and αS3 are transmembrane helices [20]. Four helices, αL2, αL4, αS1, and αS2, form a helix bundle in which a heme *b* molecule is accommodated through ligation of conserved His C131 and His D95 (Fig. 4C). Unlike the FAD molecule and the iron–sulfur centers, most residues near the heme *b* molecule are not conserved (Fig. 3C and D). A lipid molecule is bound below the heme *b* site in the helix bundle. Phosphatidylethanolamine is incorporated into the current model, although electron density patterns are not clear enough to identify the lipid species. Both heme *b* and lipid molecules are located at the interface of CybL and CybS subunits and may contribute to the assembly of the CybL and CybS subunits. Interestingly, a segment comprising 27N-terminal residues (D28–D54, Fig. 4C) of the CybS subunit extends to the Fp and Ip subunits and five residues (D29, D39, D41, D42, D46) form inter-subunit hydrogen bonds with residues of Fp (A471, A195, A192) and Ip (B150). The segment is unique to *A. suum* QFR, and seems to contribute to the stabilization of the multi-subunit structure of the enzyme. A definite cleft is formed at the interface of the Ip, CybL, and CybS subunits, and residual electron density probably revealing a bound RQ molecule is found in the cleft. The location of the cleft is in agreement with the quinone-binding sites assigned in the structures of other complex II molecules [18,21–23]. In the refined structure (3VR8), RQ is well situated in the cleft (Fig. 2) and is surrounded by residues that are highly conserved among complex II molecules from porcine, chicken and *A. suum* (Fig. 3C and D).

### 2.5. Mechanisms of fumarate reduction and rhodoquinol oxidization

The crystal structure of the fumarate-bound *A. suum* QFR (3VRB) clearly reveals that a fumarate molecule is bound to the dicarboxylate site in a non-planar conformation (Fig. 5A); C2, C3, and C4 carboxyl groups are in the same plane parallel to the FAD isoalloxazine ring but the C1 carboxyl group deviates from the plane as indicated by a C3–C2–C1–O1A dihedral angle of 83.7°. The non-planar conformation is stabilized by hydrogen bonds with conserved residues; the C1 carboxyl group with Gly A85, His A276, Thr A288, and Glu A289, and the C4 carboxyl group with Arg A320, His A387, Arg A432, and Ala A435. Accordingly, the structure suggests that the uniform distribution of π-electrons over the conjugated double bonds of fumarate is disrupted and that a partial charge separation, $C2^{\delta+}$ and $C3^{\delta-}$, is induced on the bound fumarate molecule. This charge separation seems to be the key to the reduction of fumarate because the contact of $C2^{\delta+}$ with FAD N5 (3.5 Å) observed in the crystal structure should facilitate the hydride (or hydride equivalent) transfer from reduced FAD N5 to $C2^{\delta+}$. The twisted conformation of fumarate is also observed in *E. coli* [29] and *W. succinogenes* [19] QFRs, as well as in flavoproteins such as flavocytochrome *c* [30] and *T. cruzi* dihydroorotate dehydrogenase [31], and the similar mechanism of fumarate reduction has been proposed for these enzymes. The crystal structure also suggests that conserved Arg A320 probably supplies a proton to $C3^{\delta-}$ to complete the fumarate reduction.

Fig. 5B shows the RQ binding site of *A. suum* QFR. Of 12 residues within 5 Å of the bound RQ, nine residues (B193, B194, B197, B240, B242, C72, C76, D106, and D107) are conserved in porcine, chicken, and *E. coli* SQRs (Fig. 3). The [3Fe–4S] center, the nearest iron–sulfur center to the bound RQ, is located at distances of 9.1 and 7.7 Å from RQ O1 and O2, respectively, indicating that electrons are transferred from $RQH_2$ to FAD *via* the [3Fe–4S], [4Fe–4S], and [2Fe–2S] centers. Although residues surrounding heme *b* are mostly not conserved among complex II molecules (Fig. 3), the possibility of heme *b* to act as an electron acceptor from $RQH_2$ remains because heme *b* is also the redox center close to the bound RQ (Fig. 2B) and its redox potential (−34 mV, [16]) is higher than that of $RQH_2$ (−63 mV). RQ is also surrounded by conserved amino acid residues in SQRs from porcine, chicken and *E. coli* (Ser C72, Arg C76, Asp D106, and Tyr D107) and is involved in these hydrogen bond networks: RQ O1····Tyr D107····Arg C76····Asp D106 and RQ O2····Ser C72····RQ N····Arg C76····Asp D106. Protons abstracted from $RQH_2$ can leave along these networks. It should be noted that the amino group of RQ, which is replaced by the methoxy group in ubiquinone, is involved in one of the hydrogen bond networks.

### 2.6. Flutolanil-binding site

In both crystal structures of *A. suum* QFR (Fig. 6A, 3VRB) and porcine SQR (Fig. 6B, 3AE8) complexed with flutolanil, an inhibitor specific for *A. suum* QFR [26], flutolanil is bound to the quinone-binding site located near the [3Fe–4S] center ($Q_p$ site), where residues of *A. suum* QFR and porcine SQR within 5 Å of the bound flutolanil are mostly identical (73%). The isopropoxy-phenyl moiety of flutolanil comes in contact with conserved hydrophobic residues and the carbonyl oxygen forms hydrogen bonds with tyrosine and tryptophan residues. Accordingly, these hydrogen bonds as well as van der Waals contact seem to be important for the binding of flutolanil to both enzymes. It is worth noting that there is close contact between the isopropoxy group of the bound flutolanil and the aromatic indole ring of *A. suum* QFR Trp C69; these are separated by 3.3 Å, significantly less than the distance expected for van der Waals contact (3.7 Å), indicating that they interact with each other through a C–H····π interaction. Since the tryptophan residue is replaced by methionine (Met C39) in porcine SQR, this electrostatic interaction is unique to *A. suum* QFR. Another electrostatic interaction unique to *A. suum* QFR is formed between the flutolanil trifluoromethylbenzene moiety and Arg C76 guanidino group. Since the trifluoromethyl group is an electron-withdrawing group, the π-orbital of the flutolanil aromatic ring is expected to be deficient in electrons. In contrast, the π-orbital of the guanidino group of Arg C76 seems to be rich in electrons because the arginine residue located in the hydrophobic environment of the membrane-anchoring CybL subunit may preferentially the unprotonated form over the protonated one. Therefore, the stacking of the two π-orbitals, one is deficient and another rich in electron, with the distance of 3.2 Å observed in the *A. suum* QFR-flutolanil complex reinforce the attractive interaction between flutolanil and *A. suum* QFR. In porcine SQR, however, the guanidino group of Arg C46, the counterpart residue to Arg C76, is a greater distance from the flutolanil trifluoromethylbenzene moiety and is poorly stacked.

In contrast to flutolanil, 2-thenoyltrifluoroacetone (TTFA), a potent inhibitor against mammalian SQR, does not inhibit both *A. suum* QFR and SQR [11]. There are two TTFA binding sites in porcine SQR [22], $Q_p$ and $Q_d$ sites. The $Q_p$ site TTFA, like flutolanil bound to the $Q_p$ site, accepts hydrogen bonds and van der Waals contacts from residues that, except for Trp C35 (Pro C65 in *A. suum* enzymes), are conserved in the *A. suum* enzymes, whereas the $Q_d$ site TTFA is surrounded mostly by residues unconserved in the *A. suum* enzymes and interacts with porcine SQR mainly through water molecules [22]. Therefore, if it is assumed that the $Q_p$ site is more crucial for the inhibition of complex II than the $Q_d$ site, the insensitivity of *A. suum* enzymes toward TTFA may be caused by the change from Trp C35 to Pro C65.

## 3. Twelve novel subunits of *T. cruzi* complex II

### 3.1. Subunit structure of T. cruzi complex II

The parasitic protist *T. cruzi* is the etiological agent of Chagas disease, a public health threat in Central and South America. These parasites are normally transmitted by the reduviid bug *via* vector feces after a bug bite and are also transferred *via* transfusion of infected

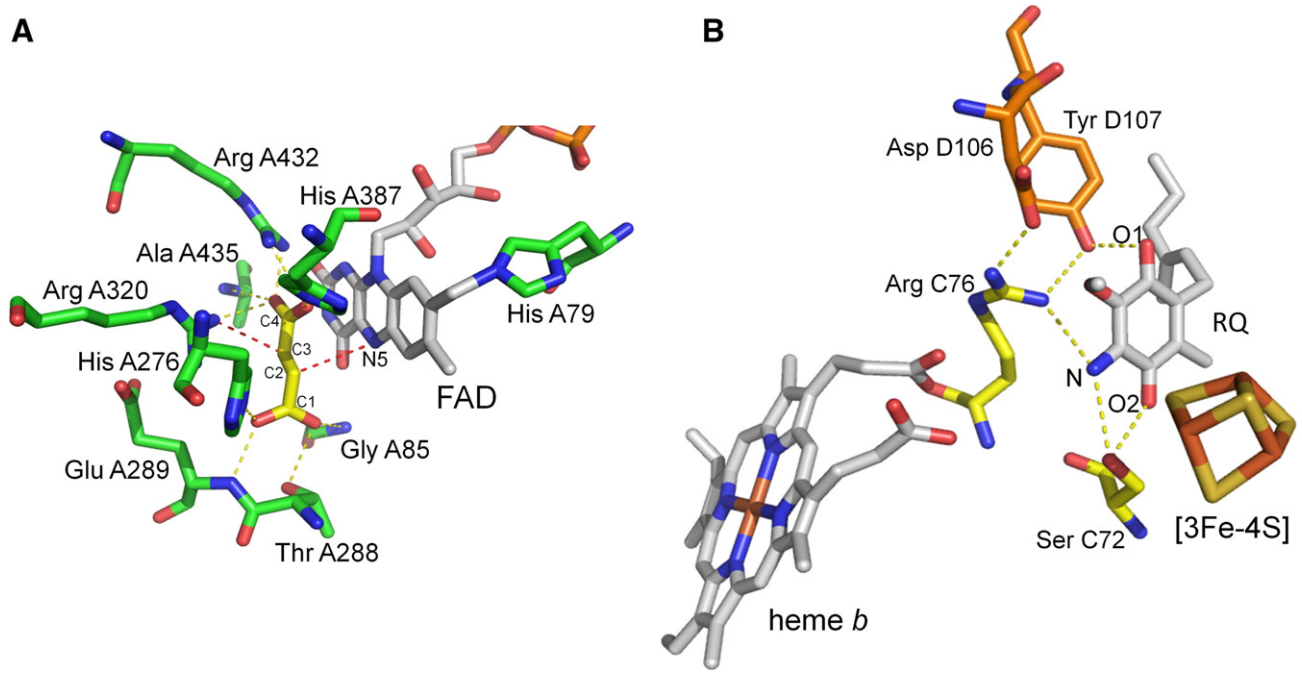


**Fig. 5.** Close-up view of active site structures. (A) The fumarate molecule bound to the dicarboxylate-binding site of *A. suum* QFR and residues interact with fumarate. Hydrogen bonds are shown in yellow dashed lines. Red dashed lines indicate probable routes of hydride (FAD N5 → fumarate $C2^{\delta+}$) and proton (Arg A320 Nη → $C3^{\delta-}$) transfers to reduce fumarate. (B) Rhodoquinol binding site of *A. suum* QFR. Hydrogen bonds are shown in yellow dashed lines. Color-coding for each atom type is as follows: N, blue; O, red; S, dark yellow; and Fe, brown. Carbon atoms of FAD, RQ and heme *b* are shown in white, residues from Fp, CybL and CybS are shown in light green, yellow, and orange, respectively.

blood. About 16 to 18 million people are infected and 100 million are at risk, but there are no definitive chemotherapeutic treatments available [32].

To our surprise, the complex II purified from *T. cruzi* consists of six hydrophilic (SDH1, $SDH2_N$, $SDH2_C$, and SDH5–SDH7) and six hydrophobic (SDH3, SDH4, and SDH8–SDH11) nuclear-encoded subunits (Fig. 7; [24]). SDH1 and SDH2 correspond to Fp (SDHA) and Ip (SDHB), respectively. Orthologous genes for each subunit were identified in most trypanosomatids, including *T. brucei* and *Leishmania major* [33–35]. Notably, the iron–sulfur subunit was heterodimeric; $SDHB_N$ and $SDHB_C$ contain the plant-type ferredoxin domain in the N-terminal half and the bacterial ferredoxin domain in the C-terminal half, respectively. Catalytic subunits (SDHA, $SDHB_N$ *plus* $SDHB_C$, SDH3, and SDH4) contain all key residues for binding of dicarboxylates and quinones, but the enzyme showed lower affinity for both substrates and inhibitors than mammalian enzymes. In addition, the enzyme binds protoheme IX, but SDH3 lacks a histidine ligand [24].

### 3.2. Split Ip subunit of Trypanosomal complex II

In contrast to the monomeric iron–sulfur subunit (SDHB) found in all known families of complex II, the Trypanosomal iron–sulfur subunit is composed of two nuclear-encoded genes for $SDHB_N$ and $SDHB_C$ subunits (Fig. 7) [24]. The crystal structure of the Ip subunit from porcine complex II [22] and the PHYRE$^2$ model [36] of *T. cruzi* $SDHB_N$ (residues $B_N66$ to $B_N161$) and $SDHB_C$ (residues $B_C34$ to $B_C163$) are shown in Fig. 8A and B, respectively. The C-terminal extension of $TcSDHB_N$ (residues $B_N162$ to $B_N270$) was removed from the model to allow better comparison between porcine Ip (Fig. 8A) and split Trypanosomal Ip (Fig. 8B) subunits. According to this model, the [2Fe–2S] center is bound to the $TcSDHB_N$ subunit (Fig. 8B) by four cysteine residues, $B_N120$, $B_N125$, $B_N128$, and $B_N140$ (Fig. 9), which correspond to cysteine residues B65, B70, B73, and B85 from porcine SDHB [22]. The [4Fe–4S] center is bound to $TcSDHB_C$ by cysteine residues $B_C71$, $B_C74$, $B_C77$, and $B_C138$ (Fig. 9), which correspond to cysteine residues B158, B161, B164, and B225 from the porcine SDHB subunit and, finally, the [3Fe–4S] center is bound by cysteine residues $B_C81$, $B_C128$, and $B_C134$ (Fig. 9), which correspond to cysteine residues B168, B215, and B221 from porcine SDHB subunit [22]. The residues from SDHB subunit which interact with flutolanil from porcine complex II (B216, B218, B169, and B173 from Fig. 4B) are also found in $TcSDHB_C$ ($B_C82$, $B_C86$, $B_C129$, and $B_C131$ in Fig. 9). Thus, even if the Ip subunit of the Trypanosomatid complex II is comprised of two distinct peptides, the three iron–sulfur clusters as well as all cysteine residues necessary to bind those clusters are structurally conserved among all families of complex II. Such spatial organization of iron–sulfur clusters is expected to be crucial for optimal electron transfer from succinate to ubiquinone.

### 3.3. T. cruzi complex II as a drug target

Purified *T. cruzi* enzyme shows reduced binding affinities for both substrates and inhibitors. Its $K_m$ values for ubiquinone ($18.8 \pm 6.4$ μM ($Q_2$)) and succinate ($1.48 \pm 0.17$ mM) were higher than those with bovine enzyme [37] (0.3 and 130 μM, respectively) and *E. coli* enzyme [38,13] (2 and 277 μM, respectively). Interestingly, the *T. cruzi* enzyme $K_m$ value for succinate was comparable to 610 μM in adult *A. suum* [10], which expresses the stage-specific complex II as QFR under hypoxic environments in the host organisms mentioned above.

Sensitivity to inhibitors also differs from that of other complex II molecules. Atpenin A5, a potent inhibitor for complex II, inhibited the *T. cruzi* enzyme with an $IC_{50}$ value of $6.4 \pm 2.4$ μM, which is three orders of magnitude higher than that of bovine enzyme (4 nM) [39]. Furthermore, *T. cruzi* enzyme does not respond to carboxin, 2-theonyltrifluoroacetone (TTFA), plumbagin, and 2-heptyl-4-hydroxyquinoline N-oxide (HQNO) (100 μM < $IC_{50}$). Structural divergence in Trypanosomatid SDH3 and SDH4 could be the cause for lower binding affinities for both quinones and inhibitors. In addition, the $IC_{50}$ for malonate (40 μM) was much higher than the $K_i$ value for bovine complex II (1.3 μM) [37], indicating different structures of the dicarboxylate-binding site.

These unusual features are unique in Trypanosomatidae and make their complex II molecules a target for new chemotherapeutic agents. Insensitivity to a known inhibitor is a promising feature for identifying a specific and potent inhibitor. Ascofuranone, which is a most

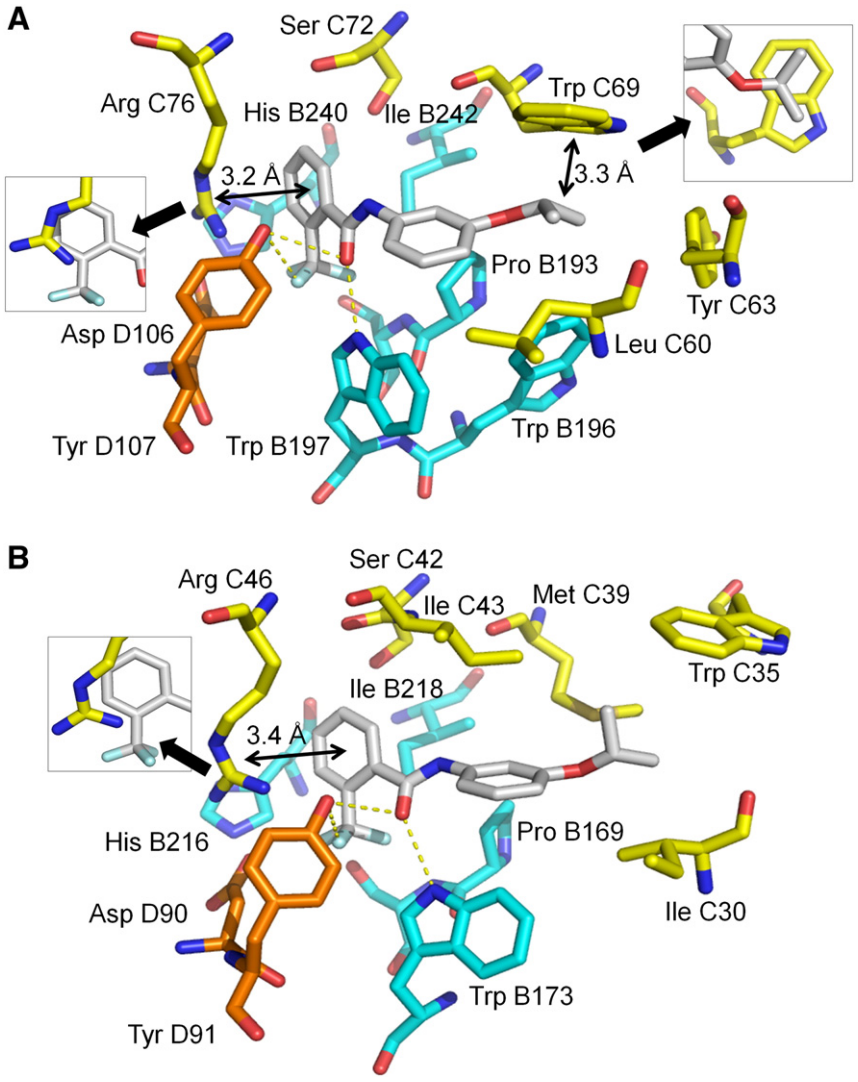


**Fig. 6.** Flutolanil binding site. The structures of flutolanil binding sites of (A) *A. suum* QFR and (B) porcine SQR. In each structure, the flutolanil molecule is bound to the quinone-binding site and surrounded by residues from Ip (cyan), CybL (yellow), and CybS (orange) subunits. Most of these residues are conserved between the two enzymes. Close-up views of the C—H·····π interaction between the isopropoxy group of flutolanil and Trp C69 side chain, and the electrostatic interaction between the flutolanil trifluoromethylbenzene moiety and Arg C76 guanidino group are shown in insets. Hydrogen bonds are shown in yellow dashed lines.

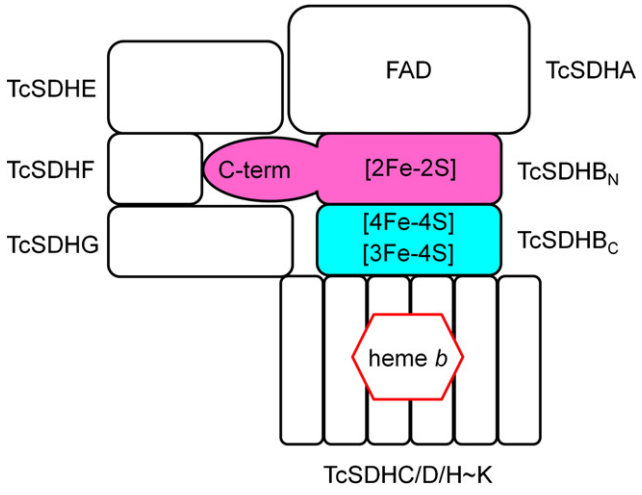


**Fig. 7.** Subunit organization model of Trypanosomal complex II. The Trypanosomal complex II is composed of six hydrophilic subunits (SDHA/$B_N$/$B_C$/E–G) and six hydrophobic subunits (SDHC/D/H–K). In the case of Trypanosomal complex II, the canonical SDHB is split into $SDHB_N$ (pink) and $SDHB_C$ (blue).

potent inhibitor of cyanide-insensitive alternative oxidase of *T. brucei* is good example [40].

## 4. Perspectives and conclusion

As described above, parasites have exploited a variety of energy-transducing systems in their adaptation to specific environments inside their hosts. Dynamic rearrangement of the respiratory chain during the life cycle is one of the key elements of this adaptation. However, the control mechanism responsible for stage-specific expression of the genes of parasites remains unclear because research on parasites at the molecular level has only recently begun. In this regard, recent reports indicating that complex II functions as an oxygen sensor are of great interest [41]. Mammalian cells are able to sense decreased oxygen availability and activate response systems, including transcriptional activation of several genes controlled via hypoxia-inducible factor-1 (HIF-1) [42]. Although the molecular mechanism of gene expression has not been elucidated for parasites, *A. suum* shows a very clear transition of the metabolic systems between larvae and adult stages, and it is, thus, a very promising research model. Our recent results show that a HIF-1 homologue plays a role in oxygen adaptation in *A. suum* and sequence analysis

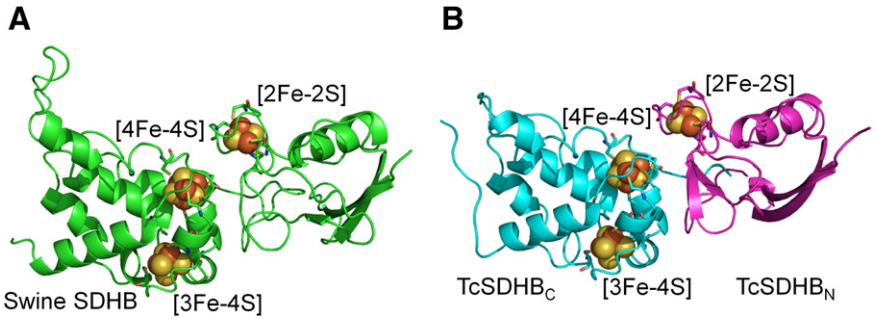


**Fig. 8.** PHYRE$^2$ model of split *T. cruzi* SDHB subunits. Superposition of porcine SDHB crystal structure (green, residues Pro B9 to Glu B237) (A), with the PHYRE$^2$ model of *T. cruzi* SDHB$_N$ (pink, residues Thr B$_N$66 to Asp B$_N$161) and SDHB$_C$ (blue, residues Val B$_C$34 to Pro B$_C$163) subunits (B). All cysteine residues coordinating with the Fe–S clusters are conserved and represented as stick, while iron (orange) and sulfur (yellow) clusters as spheres. The C-terminal residues from B$_N$162 to B$_N$270 of TcSDHB$_N$ were removed from the PHYRE$^2$ model for ease of comparison between porcine and *T. cruzi* SDHB subunits.

of the 5′-upstream regions of complex II genes identified putative hypoxia-responsive element (HREs), suggesting that HIF-1 directly regulates the expression of stage-specific complex II isoforms [43].

Diversity of complex II is found not only in parasites but also in human host. Two isoforms of human Fp, type I and type II, were reported [44,45]. These isoforms differed from each other only in two amino acid residues: Tyr 586 and Val 614 of type I Fp are replaced by Phe 586 and Ile 614 in type II Fp, respectively. Type I Fp are well conserved among the Fp of mammals, and type II Fp is found only in human complex II. Although the type I Fp gene is located on chromosome 5p15 and has an exon–intron structure [44,46], the type II Fp gene is not found in the NCBI database. Baysal et al. suggested that type II Fp is a variant of the Fp subunit and can be explained by balancing selection over the long term [47]. Interestingly, expression of type II Fp mRNA is increased in normal cells cultured under ischemic conditions [48]. It is of interest to speculate that complex II$^{II}$ has higher QFR activity and plays an important role in fumarate respiration in human mitochondria as the terminal oxidase of the system similar to that in *A. suum* adult complex II. Anti-cancer activity of pyrvinium pamoate an anthelmintic, which is a known fumarate reductase inhibitor, against human cancer cells should be studied further [49]. The diversity of mitochondrial complex II molecules lends itself to studies in many areas, including bioenergetics, molecular evolution and drug discovery.

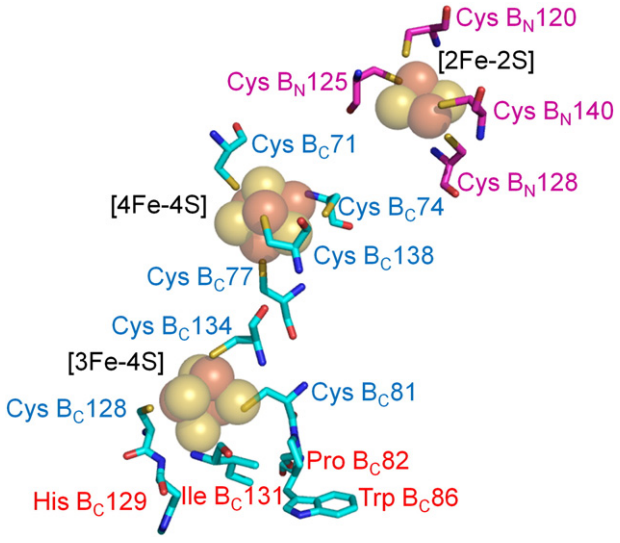


**Fig. 9.** All cysteines necessary for binding Fe–S clusters are conserved in Trypanosomal split Ip subunits. Cysteine residues from SDHB$_N$ are colored and labeled in pink and residues from SDHB$_C$ are in blue. The equivalent residues from Trypanosomal SDHB$_C$, which were found to interact with flutolanil from porcine SDHB are labeled in red. The three iron (orange) and sulfur (yellow) clusters are represented as spheres.

## Acknowledgments

This work was supported in part by Programme for the Promotion of Basic and Applied Researches for Innovations in Bio-oriented Industry (BRAIN), a Creative Scientific Research Grant 18GS0314, a Grant-in-Aid for Scientific Research on Priority Areas 18073004 from the Japanese Society for the Promotion of Science, and the Targeted Proteins Research Program of the Japanese Ministry of Education, Science, Culture, Sports and Technology (MEXT).

## References

[1] K. Kita, H. Hirawake, S. Takamiya, Cytochromes in the respiratory chain of helminth mitochondria, Int. J. Parasitol. 27 (1997) 617–630.
[2] R. Komuniecki, P.R. Komuniecki, Aerobic–anaerobic transitions in energy metabolism during the development of the parasitic nematode *Ascaris suum*, in: J.C. Boothroyd, R. Komuniecki (Eds.), Molecular Approaches to Parasitology, Wiley-Liss, Inc., New York, 1995, pp. 109–121.
[3] A.G.M. Tielens, C. Rotte, J.J. van Hellemond, W. Martin, Mitochondria as we don't know them, Trends Biochem. Sci. 27 (2002) 56–72.
[4] K. Kita, S. Takamiya, Electron-transfer complexes in *Ascaris* mitochondria, Adv. Parasitol. 51 (2002) 95–131.
[5] K. Kita, Electron-transfer complexes in *Ascaris suum*, Parasitol. Today 8 (1992) 155–159.
[6] H. Amino, A. Osanai, H. Miyadera, N. Shinjyo, E. Tomitsuka, H. Taka, R. Mineki, K. Murayama, S. Takamiya, T. Aoki, H. Miyoshi, K. Sakamoto, S. Kojima, K. Kita, Isolation and characterization of the stage-specific cytochrome *b* small subunit (Cyb*S*) of *Ascaris suum* complex II from the aerobic respiratory chain of larval mitochondria, Mol. Biochem. Parasitol. 128 (2003) 175–186.
[7] H. Amino, H. Wang, H. Hirawake, F. Saruta, D. Mizuchi, R. Mineki, N. Shindo, K. Murayama, S. Takamiya, T. Aoki, S. Kojima, K. Kita, Stage specific isoforms of *Ascaris suum* complex II: the fumarate reductase of the parasitic adult and the succinate dehydrogenase of free-living larvae share a common iron–sulfur subunit, Mol. Biochem. Parasitol. 106 (2000) 63–76.
[8] K. Kita, H. Hirawake, H. Miyadera, H. Amino, S. Takeo, Role of complex II in anaerobic respiration of the parasite mitochondria from *Ascaris suum* and *Plasmodium falciparum*, Biochim. Biophys. Acta 1553 (2002) 123–139.
[9] S. Omura, H. Miyadera, H. Ui, K. Shiomi, Y. Yamaguchi, R. Masuma, T. Nagamitsu, D. Takano, T. Sunazuka, A. Harder, H. Kölbl, M. Namikoshi, H. Miyoshi, K. Sakamoto, K. Kita, An anthelmintic compound, nafuredin, shows selective inhibition of complex I in helminth mitochondria, Proc. Natl. Acad. Sci. U. S. A. 98 (2001) 60–62.
[10] F. Saruta, T. Kuramochi, K. Nakamura, S. Takamiya, Y. Yu, T. Aoki, K. Sekimizu, S. Kojima, K. Kita, Stage-specific isoforms of complex II (succinate–ubiquinone oxidoreductase) in mitochondria from the parasitic nematode, *Ascaris suum*, J. Biol. Chem. 270 (1995) 928–932.
[11] S. Takamiya, K. Kita, H. Wang, P.P. Weinstein, A. Hiraishi, H. Oya, T. Aoki, Developmental changes in the respiratory chain of *Ascaris* mitochondria, Biochim. Biophys. Acta 1141 (1993) 65–74.
[12] S.T. Cole, C. Condon, B.D. Lemire, J.H. Weiner, Molecular biology, biochemistry and bioenergetics of fumarate reductase, a complex membrane-bound iron–sulfur flavoenzyme of *Escherichia coli*, Biochim. Biophys. Acta 811 (1985) 381–403.
[13] H. Miyadera, A. Hiraishi, H. Miyoshi, K. Sakamoto, R. Mineki, K. Murayama, K.V. Nagashima, K. Matsuura, S. Kojima, K. Kita, Complex II from phototrophic purple bacterium *Rhodoferax fermentans* displays rhodoquinol–fumarate reductase activity, Eur. J. Biochem. 270 (2003) 1863–1874.

[14] M. Heinz, Encyclopedic Reference of Parasitology, second ed. Springer, Berlin 2001.
[15] F. Iwata, N. Shinjyo, H. Amino, K. Sakamoto, M.K. Islam, N. Tsuji, K. Kita, Change of subunit composition of mitochondrial complex II (succinate-ubiquinone reductase/quinol-fumarate reductase) in *Ascaris suum* during migration in the experimental host, Parasitol. Int. 57 (2008) 54–61.
[16] C. Hägerhäll, Succinate: quinone oxidoreductases: variations on a conserved theme, Biochim. Biophys. Acta 1320 (1997) 107–141.
[17] R.S. Lemos, A.S. Fernandes, M.M. Pereira, C.M. Gomes, M. Teixeira, Quinol:fumarate oxidoreductases and succinate:quinone oxidoreductase: phylogenetic relationships, metal centres and membrane attachment, Biochim. Biophys. Acta 1553 (2002) 158–170.
[18] T.M. Iverson, C. Luna-Chavez, G. Cecchini, D.C. Rees, Structure of the *Escherichia coli* fumarate reductase respiratory complex, Science 284 (1999) 1961–1966.
[19] C.R.D. Lancaster, A. Kröger, M. Auer, H. Michel, Structure of fumarate reductase from *Wolinella succinogenes* at 2.2 Å resolution, Nature 402 (1999) 377–385.
[20] H. Shimizu, A. Osanai, K. Sakamoto, D.K. Inaoka, T. Shiba, S. Harada, K. Kita, Crystal structure of mitochondrial quinol–fumarate reductase from the parasitic nematode *Ascaris suum*, J. Biochem. 151 (2012) 589–592.
[21] V. Yankovskaya, R. Horsefield, S. Törnroth, C. Luna-Chavez, H. Miyoshi, C. Léger, B. Byrne, G. Cecchini, S. Iwata, Architecture of succinate dehydrogenase and reactive oxygen species generation, Science 299 (2003) 700–704.
[22] F. Sun, X. Huo, Y. Zhai, A. Wang, J. Xu, D. Su, M. Bartlam, Z. Rao, Crystal structure of mitochondrial respiratory membrane protein complex II, Cell 121 (2005) 1043–1057.
[23] L. Huang, G. Sun, D. Cobessi, A.C. Wang, J.T. Shen, E.Y. Tung, V.E. Anderson, E.A. Berry, 3-Nitropropionic acid is a suicide inhibitor of mitochondrial respiration that, upon oxidation by complex II, forms a covalent adduct with a catalytic base arginine in the active site of the enzyme, J. Biol. Chem. 281 (2006) 5965–5972.
[24] J. Morales, T. Mogi, S. Mineki, E. Takashima, R. Mineki, H. Hirawake, K. Sakamoto, S. Ōmura, K. Kita, Novel mitochondrial complex II isolated from *Trypanosoma cruzi* is composed of twelve peptides including a heterodimeric Ip subunit, J. Biol. Chem. 284 (2009) 7255–7263.
[25] T. Mogi, K. Kita, Identification of mitochondrial complex II subunits SDH3 and SDH4 and ATP synthase subunits a and b in *Plasmodium* spp, Mitochondrion 9 (2009) 443–453.
[26] A. Osanai, S. Harada, K. Sakamoto, H. Shimizu, D.K. Inaoka, K. Kita, Crystallization of mitochondrial rhodoquinol-fumarate reductase from the parasitic nematode *Ascaris suum* with the specific inhibitor flutolanil, Acta Crystallogr., Sect. F: Struct. Biol. Cryst. Commun. 65 (2009) 941–944.
[27] K. Motoba, M. Uchida, E. Tada, Mode of antifungal action and selectivity of flutolanil, Agric. Biol. Chem. 52 (1988) 1445–1449.
[28] C.C. Page, C.C. Moser, X. Chen, P.L. Dutton, Natural engineering principles of electron tunnelling in biological oxidation-reduction, Nature 402 (1999) 47–52.
[29] T.M. Tomasiak, T.L. Archuleta, J. Andrell, C. Luna-Chavez, T.A. Davis, M. Sarwar, A.J. Ham, W.H. McDonald, V. Yankovskaya, H.A. Stern, J.N. Johnston, E. Maklashina, G. Cecchini, T.M. Iverson, Geometric restraint drives on- and off-pathway catalysis by the *Escherichia coli* menaquinol:fumarate reductase, J. Biol. Chem. 286 (2011) 3047–3056.
[30] P. Taylor, S.L. Pealing, G.A. Reid, S.K. Chapman, M.D. Walkinshaw, Structural and mechanistic mapping of a unique fumarate reductase, Nat. Struct. Biol. 6 (1999) 1108–1112.
[31] D.K. Inaoka, K. Sakamoto, H. Shimizu, T. Shiba, G. Kurisu, T. Nara, T. Aoki, K. Kita, S. Harada, Structures of *Trypanosoma cruzi* dihydroorotate dehydrogenase complexed with substrates and products: atomic resolution insights into mechanisms of dihydroorotate oxidation and fumarate reduction, Biochemistry 47 (2008) 10881–10891.
[32] World Health Organization Report of the first meeting of WHO Strategic and Technical Advisory Group on Neglected Tropical Diseases, WHO, Geneva, Switzerland, 2007.
[33] N.M. El-Sayed, P.J. Myler, D.C. Bartholomeu, D. Nilsson, G. Aggarwal, A.N. Tran, E. Ghedin, E.A. Worthey, A.L. Delcher, G. Blandin, S.J. Westenberger, E. Caler, G.C. Cerqueira, C. Branche, B. Haas, A. Anupama, E. Arner, L. Aslund, P. Attipoe, E. Bontempi, F. Bringaud, P. Burton, E. Cadag, D.A. Campbell, M. Carrington, J. Crabtree, H. Darban, J.F. da Silveira, P. de Jong, K. Edwards, P.T. Englund, G. Fazelina, T. Feldblyum, M. Ferella, A.C. Frasch, K. Gull, D. Horn, L. Hou, Y. Huang, E. Kindlund, M. Klingbeil, S. Kluge, H. Koo, D. Lacerda, M.J. Levin, H. Lorenzi, T. Louie, C.R. Machado, R. McCulloch, A. McKenna, Y. Mizuno, J.C. Mottram, S. Nelson, S. Ochaya, K. Osoegawa, G. Pai, M. Parsons, M. Pentony, U. Pettersson, M. Pop, J.L. Ramirez, J. Rinta, L. Robertson, S.L. Salzberg, D.O. Sanchez, A. Seyler, R. Sharma, J. Shetty, A.J. Simpson, E. Sisk, M.T. Tammi, R. Tarleton, S. Teixeira, S. Van Aken, C. Vogt, P.N. Ward, B. Wickstead, J. Wortman, O. White, C.M. Fraser, K.D. Stuart, B. Andersson, The genome sequence of *Trypanosoma cruzi*, etiologic agent of Chagas disease, Science 309 (2005) 409–415.
[34] M. Berriman, E. Ghedin, C. Hertz-Fowler, G. Blandin, H. Renauld, D.C. Bartholomeu, N.J. Lennard, E. Caler, N.E. Hamlin, B. Haas, U. Böhme, L. Hannick, M.A. Aslett, J. Shallom, L. Marcello, L. Hou, B. Wickstead, U.C. Alsmark, C. Arrowsmith, R.J. Atkin, A.J. Barron, F. Bringaud, K. Brooks, M. Carrington, I. Cherevach, T.J. Chillingworth, C. Churcher, L.N. Clark, C.H. Corton, A. Cronin, R.M. Davies, J. Doggett, A. Djikeng, T. Feldblyum, M.C. Field, A. Fraser, I. Goodhead, Z. Hance, D. Harper, B.R. Harris, H. Hauser, J. Hostetler, A. Ivens, K. Jagels, D. Johnson, J. Johnson, K. Jones, A.X. Kerhornou, H. Koo, N. Larke, S. Landfear, C. Larkin, V. Leech, A. Line, A. Lord, A. Macleod, P.J. Mooney, S. Moule, D.M. Martin, G.W. Morgan, K. Mungall, H. Norbertczak, D. Ormond, G. Pai, C.S. Peacock, J. Peterson, M.A. Quail, E. Rabbinowitsch, M.A. Rajandream, C. Reitter, S.L. Salzberg, M. Sanders, S. Schobel, S. Sharp, M. Simmonds, A.J. Simpson, L. Tallon, C.M. Turner, A. Tait, A.R. Tivey, S. Van Aken, D. Walker, D. Wanless, S. Wang, B. White, O. White, S. Whitehead, J. Woodward, J. Wortman, M.D. Adams, T.M. Embley, K. Gull, E. Ullu, J.D. Barry, A.H. Fairlamb, F. Opperdoes, B.G. Barrell, J.E. Donelson, N. Hall, C.M. Fraser, S.E. Melville, N.M. El-Sayed, The genome of the African trypanosome *Trypanosoma brucei*, Science 309 (2005) 416–422.
[35] A.C. Ivens, C.S. Peacock, E.A. Worthey, L. Murphy, G. Aggarwal, M. Berriman, E. Sisk, M.A. Rajandream, E. Adlem, R. Aert, A. Anupama, Z. Apostolou, P. Attipoe, N. Bason, C. Bauser, A. Beck, S.M. Beverley, G. Bianchettin, K. Borzym, G. Bothe, C.V. Bruschi, M. Collins, E. Cadag, L. Ciarloni, C. Clayton, R.M. Coulson, A. Cronin, A.K. Cruz, R.M. Davies, J. De Gaudenzi, D.E. Dobson, A. Duesterhoeft, G. Fazelina, N. Fosker, A.C. Frasch, A. Fraser, M. Fuchs, C. Gabel, A. Goble, A. Goffeau, D. Harris, C. Hertz-Fowler, H. Hilbert, D. Horn, Y. Huang, S. Klages, A. Knights, M. Kube, N. Larke, L. Litvin, A. Lord, T. Louie, M. Marra, D. Masuy, K. Matthews, S. Michaeli, J.C. Mottram, S. Müller-Auer, H. Munden, S. Nelson, H. Norbertczak, K. Oliver, S. O'neil, M. Pentony, T.M. Pohl, C. Price, B. Purnelle, M.A. Quail, E. Rabbinowitsch, R. Reinhardt, M. Rieger, J. Rinta, J. Robben, L. Robertson, J.C. Ruiz, S. Rutter, D. Saunders, M. Schäfer, J. Schein, D.C. Schwartz, K. Seeger, A. Seyler, S. Sharp, H. Shin, D. Sivam, R. Squares, S. Squares, V. Tosato, C. Vogt, G. Volckaert, R. Wambutt, T. Warren, H. Wedler, J. Woodward, S. Zhou, W. Zimmermann, D.F. Smith, J.M. Blackwell, K.D. Stuart, B. Barrell, P.J. Myler, The genome of the kinetoplastid parasite, *Leishmania major*, Science 309 (2005) 436–442.
[36] L.A. Kelley, M.J. Sternberg, Protein structure prediction on the Web: a case study using the Phyre server, Nat. Protoc. 4 (2009) 363–371.
[37] V.G. Grivennikova, E.V. Gavrikova, A.A. Timoshin, A.D. Vinogradov, Fumarate reductase activity of bovine heart succinate-ubiquinone reductase. New assay system and overall properties of the reaction, Biochim. Biophys. Acta 1140 (1993) 282–292.
[38] E. Maklashina, G. Cecchini, Comparison of catalytic activity and inhibitors of quinone reactions of succinate dehydrogenase (Succinate-ubiquinone oxidoreductase) and fumarate reductase (Menaquinol-fumarate oxidoreductase) from *Escherichia coli*, Arch. Biochem. Biophys. 369 (1999) 223–232.
[39] H. Miyadera, K. Shiomi, H. Ui, Y. Yamaguchi, R. Masuma, H. Tomoda, H. Miyoshi, A. Osanai, K. Kita, S. Omura, Atpenins, potent and specific inhibitors of mitochondrial complex II (succinate-ubiquinone oxidoreductase), Proc. Natl. Acad. Sci. U. S. A. 100 (2003) 473–477.
[40] Y. Kido, K. Sakamoto, K. Nakamura, M. Harada, T. Suzuki, Y. Yabu, H. Saimoto, F. Yamakura, D. Ohmori, A. Moore, S. Harada, K. Kita, Purification and kinetic characterization of recombinant alternative oxidase from *Trypanosoma brucei brucei*, Biochim. Biophys. Acta 1797 (2010) 443–450.
[41] B.E. Baysal, R.E. Ferrell, J.E. Willett-Brozick, E.C. Lawrence, D. Myssiorek, A. Bosch, A. van der Mey, P.E. Taschner, W.S. Rubinstein, E.N. Myers, C.W. Richard, C.J. Cornelisse, P. Devilee, B. Devlin, Mutations in SDHD, a mitochondrial complex II gene, in hereditary paraganglioma, Science 287 (2000) 848–851.
[42] G.L. Semenza, Oxygen sensing, homeostasis, and disease, N. Engl. J. Med. 365 (2011) 537–547.
[43] M. Goto, H. Amino, M. Nakajima, N. Tsuji, K. Sakamoto, K. Kita, Cloning and characterization of hypoxia-inducible factor-1 subunits from *Ascaris suum* - a parasitic nematode highly adapted to changes of oxygen conditions during its life cycle, Gene (in press), http://dx.doi.org/10.1016/j.gene.2012.12.025.
[44] E. Tomitsuka, H. Hirawake, Y. Goto, M. Taniwaki, S. Harada, K. Kita, Direct evidence for two distinct forms of the flavoprotein subunit of human mitochondrial complex II (succinate-ubiquinone reductase), J. Biochem. 134 (2003) 191–195.
[45] E. Tomitsuka, Y. Goto, M. Taniwaki, K. Kita, Direct evidence for expression of type II flavoprotein subunit in human complex II (succinate-ubiquinone reductase), Biochem. Biophys. Res. Commun. 311 (2003) 774–779.
[46] T. Bourgeron, P. Rustin, D. Chretien, M. Birch-Machin, M. Bourgeois, E. Viegas-Péquignot, A. Munnich, A. Rötig, Mutation of a nuclear succinate dehydrogenase gene results in mitochondrial respiratory chain deficiency, Nat. Genet. 11 (1995) 144–149.
[47] B.E. Baysal, E.C. Lawrence, R.E. Ferrell, Sequence variation in human succinate dehydrogenase genes: evidence for long-term balancing selection on SDHA, BMC Biol. 5 (2007) 12.
[48] C. Sakai, E. Tomitsuka, H. Esumi, S. Harada, K. Kita, Mitochondrial fumarate reductase as a target of chemotherapy: from parasites to cancer cells, Biochim. Biophys. Acta 1820 (2012) 643–651.
[49] E. Tomitsuka, K. Kita, H. Esumi, An anticancer agent, pyrvinium pamoate inhibits the NADH-fumarate reductase system—a unique mitochondrial energy metabolism in tumour microenvironments, J. Biochem. 152 (2012) 171–183.